Steel and Composite Structures, *Vol. 28, No. 4 (2018) 495-508*
DOI: https://doi.org/10.12989/scs.2018.28.4.495

Characterizing buckling behavior of matrix-cracked hybrid plates containing CNTR-FG layers

Zuxiang Lei * and Yang Zhang

School of Sciences, Nanjing University of Science and Technology, Nanjing 210094, China

(*Received April 30, 2018, Revised June 6, 2018, Accepted June 11, 2018*)

Abstract. In this paper, the effect of matrix cracks on the buckling of a hybrid laminated plate is investigated. The plate is composed of carbon nanotube reinforced functionally graded (CNTR-FG) layers and conventional fiber reinforced composite (FRC) layers. Different distributions of single walled carbon nanotubes (SWCNTs) through the thickness of layers are considered. The cracks are modeled as aligned slit cracks across the ply thickness and transverse to the laminate plane, and the distribution of cracks is assumed statistically homogeneous corresponding to an average crack density. The first-order shear deformation theory (FSDT) is employed to incorporate the effects of rotary inertia and transverse shear deformation, and the meshless kp-Ritz method is used to obtain the buckling solutions. Detailed parametric studies are conducted to investigate the effects of matrix crack density, CNTs distributions, CNT volume fraction, plate aspect ratio and plate length-to-thickness ratio, boundary conditions and number of layers on buckling behaviors of hybrid laminated plates containing CNTR-FG layers.

Keywords: buckling; carbon nanotube-reinforced functionally graded composites; matrix crack; meshless kp-Ritz method

1. Introduction

Due to cyclic loads or environmental effects, internal matrix cracks and delamination may develop in laminated structures at strain levels well below the failure strain. These cracks lead to the main low-stress damage modes that are the main cause of reduction in the stiffness and strength. For the design of laminated composites, the effect of matrix cracking needs to be considered, which is likely to cause the changes of stiffness.

Budiansky and O'Connell (1976) reported a noteworthy study of solids with cracks by developing a self-consistent model to compute the elastic moduli of cracked isotropic solids. Laws and Dvorak (1988) proposed a shear-lag model to investigate the progressive transverse cracking of the matrix. Lee and Daniel (1990) proposed a simplified shear lag analysis using a progressive damage scheme for cross-ply composite laminates under uniaxial tensile loading. Gudmundson and Weilin (1993) presented an analytical model for the prediction of the thermoelastic properties of composite laminates containing matrix cracks which is parallel to the fiber direction or perpendicular to the laminate plane. For delaminated composite plates, Nikrad and Asadi (2015) examined the thermal instability and thermal postbuckling of rectangular delaminated composite plates by taking into consideration the von Karman geometrical nonlinearity. Nikrad *et al*. (2017) investigated the mechanical stability of L-section and T-section composite struts with single edge delamination. With considering off-center delaminations, the postbuckling behavior and the delamination growth of geometrically imperfect composite plates was studied by Nikrad *et al*. (2016). Kashtalyan and Soutis (2013) described an analytical approach to predict the effect of intra- (matrix cracking and splitting) and inter-laminar (delamination) damage on the residual stiffness properties of the laminate, which can be used in the post-initial failure analysis, taking full account of damage mode interaction. Gayathri *et al*. (2010) presented static and dynamic analysis of a laminated composite plate model based on first order shear deformation theory with matrix cracks introduced into the finite element model by considering changes in the different matrices of composites. Makins and Adali (1991) presented a bending analysis for cross-ply laminates containing matrix cracks which are assumed to be statistically homogeneous corresponding to an average crack density. The effect of matrix cracks on the buckling of unsymmetrical, cross-ply laminates is investigated in Adali and Makins (1991).

Numerous studies showed that carbon nanotubes (CNTs) have excellent mechanical, electrical and thermal properties. Many studies have been presented about mechanical properties of single layer CNT-reinforced composite beams, plates and shells Mehri *et al*. (2016a, b), Asadi (2017), Asadi *et al*. (2017), Asadi and Wang (2017a, b), Mehri *et al*. (2017). Disparate the above-mentioned studies, only limited work has been reported on the laminated CNTR-FG composite plates. For static analysis laminated FG-CNT reinforced composite rectangular plates, detailed stress analysis is presented in Lei *et al*. (2016a). Bahrami *et al*. (2018) examined the in-plane and out-of-plane forced vibration of a curved nanocomposite

∗Corresponding author, Ph.D., Associate Professor,
E-mail: leizux@njust.edu.cn

http://www.techno-press.org/?journal=scs&subpage=6
ISSN: 1229-9367 (Print), 1598-6233 (Online)

microbeam. Using the element-free kp-Ritz method, Ebrahimi and Farazmandnia (2018) presented thermo-mechanical buckling of sandwich beams with a stiff core and face sheets made of functionally graded carbon nanotube-reinforced composite (FG-CNTRC) within the framework of Timoshenko beam theory. With CNTR-FG composite structures integrated with piezoelectric layers, the mechanical properties of vibration, and postbuckling were studied in detail by Keleshteri *et al.* (2017a, b), Mohammadzadeh-Keleshteri *et al*. (2017), Keleshteri *et al*. (2018). Arani *et al*. (2018) investigated buckling and free vibration analysis of sandwich micro plate (SMP) integrated with piezoelectric layers embedded in orthotropic Pasternak. Moradi-Dastjerdi and Payganeh (2017) studied thermoelastic dynamic behavior of functionally graded carbon nanotube reinforced composite (FG-CNTRC) cylinders subjected to mechanical pressure loads, uniform temperature environment or thermal gradient loads. Tahouneh (2018) examined free vibration characteristics of sandwich sectorial plates with multiwalled carbon nanotube-(MWCNT)-reinforced composite core. For CNT reinforced functionally graded rotating laminated cylindrical panels, a parametric analysis of frequency is presented in Lei *et al*. (2016b).

This paper presented the buckling analysis of a hybrid laminated plate with matrix cracks. In this study, the laminated plate is composed of perfectly bonded with carbon nanotube reinforced functionally graded (CNTR-FG) layers and conventional fiber reinforced composite (FRC) layers. In CNTR-FG layers, the CNTs is uniformly distributed or functionally graded in the thickness direction. A self-consistent model is employed to describe the stiffness reduction due to the matrix cracking. The governing eigenvalue equation for buckling analysis is derived based on the first-order shear deformation theory (FSDT) and the kernel particle approximation via the Ritz procedure. The numerical illustrations show the influences of matrix crack density, CNTs distributions, CNT volume fraction, plate aspect ratio and plate length-to-thickness ratio, boundary conditions and number of layers on buckling behaviors of hybrid laminated plates containing CNTR-FG layers.

2. Problem definition

In this study, a hybrid laminated composite plate composed of perfectly bonded CNTR-FG layers and FRC layers with thickness t and N layers, as shown in Fig. 1. N is the total number of layers and each layer has thickness h_0. For each CNTR-FG layer, three types of distributions of CNT are considered. UD represents the uniform distribution and FG-O and FG-X denote the other two functionally graded distributions. The hybrid laminated plate has length a, width b, thickness t, with an arbitrary combination of boundary conditions along the four edges.

2.1 Material properties of FRC layers

A micromechanical model is introduced to describe the material properties of a FRC layer by Shen (2009a)

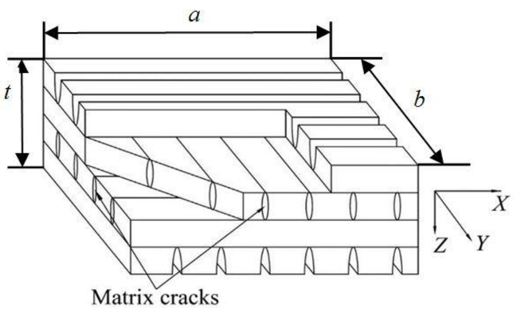

Fig. 1 Geometry of a hybrid laminated composite plate composed of perfectly bonded CNTR-FG layers and FRC layers

$$E_{11} = V_f E_{11}^f + V_m E^m \tag{1}$$

$$\frac{1}{E_{22}} = \frac{V_f}{E_{22}^f} + \frac{V_m}{E^m} - V_f V_m \frac{V_f^2 E^m / E_{22}^f + V_m^2 E_{22}^f E^m / E^m}{V_f E_{22}^f + V_m E^m} \tag{2}$$

$$\frac{1}{G_{ij}} = \frac{V_f}{G_{ij}^f} + \frac{V_m}{G_m} \quad (ij = 12, 13 \text{ and } 23) \tag{3}$$

$$\nu_{12} = V_f \nu^f + V_m \nu^m \tag{4}$$

where E_{11}^f, E_{22}^f, G_{ij}^f and v^f are the Young's moduli, shear moduli and Poisson's ratio of the fiber, while E^m, G^m and v^m are corresponding properties for the matrix. V_f and V_m are the fiber and matrix volume fractions.

2.2 Material properties of CNTR-FG layers

Distributions of CNTs along the thickness direction of each CNTR-FG layer are given as

$$V_{CNT}(z) = \begin{cases} V_{CNT}^* & (\text{UD} \quad CNTR-FG) \\ 2\left(1 - \dfrac{2|z|}{h_0}\right) V_{CNT}^* & (\text{FG-O } CNTR-FG) \\ 2\left(\dfrac{2|z|}{h_0}\right) V_{CNT}^* & (\text{FG-X } CNTR-FG) \end{cases} \tag{5}$$

It is assumed the CNTR-FG laminated plates are made of a mixture of SWCNTs and an isotropic matrix. The following material properties for the matrix are used: $v_m = 0.34$, $\alpha^m = 45(1 + 0.0005\Delta T) \times 10^{-6}/K$ and $E^m = (3.52 - 0.0034T)$ GPa, where $T = T_0 + \Delta T$ and $T_0 = 300$ K (room temperature). The CNTs selected in this paper are the type of armchair (10,10) SWCNTs with material properties: $E_{11}^{CNT} = 5.6466\, TPa$, $G_{22}^{CNT} = 7.0800\, TPa$. According to the extended rule of mixture of Shen (2009b), the effective material properties of CNTR-FG layer can be expressed as

$$E_{11} = \eta_1 V_{\mathrm{CNT}} E_{11}^{\mathrm{CNT}} + V_{\mathrm{m}} E^{\mathrm{m}} \tag{6}$$

$$\frac{\eta_2}{E_{22}} = \frac{V_{CNT}}{E_{22}^{CNT}} + \frac{V_m}{E^m} \tag{7}$$

$$\frac{\eta_3}{G_{12}} = \frac{V_{CNT}}{G_{12}^{CNT}} + \frac{V_m}{G^m} \tag{8}$$

where E_{11}^{CNT}, E_{22}^{CNT} and G_{12}^{CNT} are the Young's moduli and shear modulus of SWCNTs, respectively, and E_m and G_m are the corresponding properties of the isotropic matrix. η_j $(j = 1, 2, 3)$, the CNT efficiency parameters are calculated by matching the effective properties obtained from the MD simulations with those from the rule of mixture.

Also, using the rule of mixture, thermal expansion coefficients, Poisson's ratio and the density can be calculated as

$$\nu_{12} = V_{CNT}^{*} \nu_{12}^{CNT} + V_m \nu^m \tag{9}$$

$$\rho = V_{CNT} \rho^{CNT} + V_m \rho^m \tag{10}$$

where v_{12}^{CNT} and v^m are Poisson's ratios of the CNT and matrix, respectively.

2.3 Modeling for matrix cracks

On the macro-scale, the cracked unidirectional composite of Fig. 1 can be regarded as an orthotropic homogeneous solid. The elastic properties of the matrix are identical with those of the fibrous composite and can be easily evaluated. When cracks are introduced, the macroscopic or overall elastic moduli of the solid are changed. According to Laws *et al*. (1983), with the cracks are introduced, the self-consistent estimates for the overall compliance matrices S can be given as

$$\boldsymbol{S} = \boldsymbol{S}_0 + \bar{\beta}\Lambda \tag{11}$$

where

$$\bar{\beta} = \frac{1}{4}\pi\beta \tag{12}$$

in which β is the crack density parameter which is defined by Ref. Dvorak *et al*. (1985).

The matrix Λ has only three nonzero components, which are expressed in terms of compliances S_{ij} as

$$\Lambda_{22} = \frac{S_{11}S_{22} - S_{12}^2}{S_{11}} (\alpha_1^{1/2} + \alpha_2^{1/2}) \tag{13}$$

$$\Lambda_{44} = \frac{(S_{11}S_{22} - S_{12}^2)^{1/2}(S_{11}S_{33} - S_{13}^2)^{1/2}}{S_{11}} (\alpha_1^{1/2} + \alpha_2^{1/2}) \tag{14}$$

$$\Lambda_{66} = S_{55}^{1/2} S_{66}^{1/2} \tag{15}$$

where α_1 and α_2 are roots of the following equation

$$\begin{aligned}&(S_{11}S_{22} - S_{12}^2)\alpha^2 - [S_{11}S_{44} + 2(S_{11}S_{23} - S_{12}S_{13})]\alpha \\ &+ S_{11}S_{33} - S_{13}^2 = 0\end{aligned} \tag{16}$$

These results imply that only three compliance coefficients S_{22}, S_{44}, and S_{66} are affected by the introduction of cracks, the remaining six terms in $\boldsymbol{S}$ are unchanged, i.e., they remain equal to those of the uncracked fiber composite.

In particular

$$S_{11} = S_{11}^0,\ S_{12} = S_{12}^0,\ S_{13} = S_{13}^0 \tag{17}$$

$$S_{23} = S_{23}^0,\ S_{33} = S_{33}^0,\ S_{55} = S_{55}^0 \tag{18}$$

$$S_{22} = S_{22}^0 + \bar{\beta}\frac{S_{11}S_{22} - S_{12}^2}{S_{11}} (\alpha_1^{1/2} + \alpha_2^{1/2}) \tag{19}$$

$$S_{44} = S_{44}^0 + \bar{\beta}\frac{(S_{11}S_{22} - S_{12}^2)^{1/2}(S_{11}S_{33} - S_{13}^2)^{1/2}}{S_{11}} (\alpha_1^{1/2} + \alpha_2^{1/2}) \tag{20}$$

$$S_{66} = S_{66}^0 + \bar{\beta} S_{55}^{1/2} S_{66}^{1/2} \tag{21}$$

Once the values of S_{ij} are computed, the reduced stiffness components Q_{ij} are obtained by inverting the compliance matrix.

3. Theoretical formulations

3.1 Energy formulation

Based on the FSDT, the displacement field is defined as

$$\begin{Bmatrix} u(x,y,z) \\ v(x,y,z) \\ w(x,y,z) \end{Bmatrix} = \begin{Bmatrix} u_0(x,y) \\ v_0(x,y) \\ w_0(x,y) \end{Bmatrix} + z \cdot \begin{Bmatrix} \varphi_x(x,y) \\ \varphi_y(x,y) \\ 0 \end{Bmatrix} \tag{22}$$

where u_0, v_0 and w_0 denote the translation displacements of a point at the mid-plane, respectively; φ_x and φ_y represents rotations of a transverse normal about positive y and negative x axes. The linear strain-displacement relationships are given by

$$\begin{Bmatrix} \varepsilon_{xx} \\ \varepsilon_{yy} \\ \gamma_{xy} \end{Bmatrix} = \boldsymbol{\varepsilon}_0 + z\boldsymbol{\kappa},\ \begin{Bmatrix} \gamma_{yz} \\ \gamma_{xz} \end{Bmatrix} = \boldsymbol{\gamma}_0 \tag{23}$$

where

$$\boldsymbol{\varepsilon}_0 = \begin{Bmatrix} \dfrac{\partial u_0}{\partial x} \\ \dfrac{\partial v_0}{\partial y} \\ \dfrac{\partial u_0}{\partial y} + \dfrac{\partial v_0}{\partial x} \end{Bmatrix},\ \boldsymbol{\kappa} = \begin{Bmatrix} \dfrac{\partial \theta_x}{\partial x} \\ \dfrac{\partial \theta_y}{\partial y} \\ \dfrac{\partial \theta_x}{\partial y} + \dfrac{\partial \theta_y}{\partial x} \end{Bmatrix},\ \boldsymbol{\gamma}_0 = \begin{Bmatrix} \theta_y + \dfrac{\partial w_0}{\partial y} \\ \theta_x + \dfrac{\partial w_0}{\partial x} \end{Bmatrix} \tag{24}$$

The linear constitutive relations are expressed as

$$\begin{Bmatrix} \sigma_{xx} \\ \sigma_{yy} \\ \sigma_{xy} \\ \sigma_{yz} \\ \sigma_{xz} \end{Bmatrix} = \begin{bmatrix} Q_{11} & Q_{12} & 0 & 0 & 0 \\ Q_{12} & Q_{22} & 0 & 0 & 0 \\ 0 & 0 & Q_{66} & 0 & 0 \\ 0 & 0 & 0 & Q_{44} & 0 \\ 0 & 0 & 0 & 0 & Q_{55} \end{bmatrix} \begin{Bmatrix} \varepsilon_{xx} \\ \varepsilon_{yy} \\ \gamma_{xy} \\ \gamma_{yz} \\ \gamma_{xz} \end{Bmatrix} \tag{25}$$

where

$$Q_{11} = \frac{E_{11}}{1-\nu_{12}\nu_{21}},\ Q_{22} = \frac{E_{22}}{1-\nu_{12}\nu_{21}},\ Q_{12} = \frac{\nu_{21}E_{11}}{1-\nu_{12}\nu_{21}} \tag{26}$$

$$Q_{66} = G_{12},\ Q_{44} = G_{23},\ Q_{55} = G_{13} \tag{27}$$

and ΔT is the temperature change, E_{11} and E_{22} are effective Young's moduli of hybrid laminated plates; G_{12}, G_{13} and G_{23} are the shear moduli; α_{11} and α_{22} are the thermal expansion coefficients; and ν_{12} and ν_{21} are the Poisson's ratios.

The strain energy of the hybrid laminated plates is given by

$$U_\varepsilon = \frac{1}{2}\int_\Omega \boldsymbol{\varepsilon}^{\mathrm{T}}\mathbf{S}\boldsymbol{\varepsilon}\mathrm{d}\Omega \tag{28}$$

where

$$\boldsymbol{\varepsilon} = \begin{Bmatrix} \boldsymbol{\varepsilon_0} \\ \boldsymbol{\kappa} \\ \boldsymbol{\gamma_0} \end{Bmatrix},\ \mathbf{S} = \begin{bmatrix} \mathbf{A} & \bar{\mathbf{B}} & \mathbf{0} \\ \bar{\mathbf{B}} & \mathbf{D} & \mathbf{0} \\ \mathbf{0} & \mathbf{0} & \mathbf{A}_s \end{bmatrix} \tag{29}$$

in which

$$(A_{ij}, B_{ij}, D_{ij}) = \int_{-h/2}^{h/2} Q_{ij}(1, z, z^2)\mathrm{d}z,\ A_{ij}^s = K\int_{-h/2}^{h/2} Q_{ij}\mathrm{d}z \tag{30}$$

where K is the transverse shear correction coefficient, which is suggested as $K = 5 / (6 - (\nu_1 V_1 + \nu_2 V_2))$ for FGMs Efraim and Eisenberger (2007).

For a laminated plate, the stiffnesses can be expressed as

$$\begin{aligned} A_{ij} &= \sum_{k=1}^{N}\int_{t_k}^{t_{k+1}} \bar{Q}_{ij}^k \mathrm{d}z \\ B_{ij} &= \sum_{k=1}^{N}\int_{t_k}^{t_{k+1}} \bar{Q}_{ij}^k z\mathrm{d}z \\ D_{ij} &= \sum_{k=1}^{N}\int_{t_k}^{t_{k+1}} \bar{Q}_{ij}^k z^2\mathrm{d}z \end{aligned} \tag{31}$$

where $\bar{Q}_{ij}^k$ is the transformed reduced stiffness matrix for the kth layer where

$$[\bar{Q}] = [T]^{-1}[Q][T]^{-T} \tag{32}$$

and $[T]$ is the transformation matrix, and is given as

$$[T] = \begin{bmatrix} \cos^2\theta & \sin^2\theta & 2\cos\theta\sin\theta & 0 & 0 \\ \sin^2\theta & \cos^2\theta & -2\cos\theta\sin\theta & 0 & 0 \\ -\cos\theta\sin\theta & \cos\theta\sin\theta & \cos^2\theta - \sin^2\theta & 0 & 0 \\ 0 & 0 & 0 & \cos\theta & -\sin\theta \\ 0 & 0 & 0 & \sin\theta & \cos\theta \end{bmatrix} \tag{33}$$

where θ is the lamination angle.

The potential energy due to in-plane loads is given by

$$W_g = \int_\Omega \frac{1}{2}\begin{bmatrix} \dfrac{\partial w}{\partial x} & \dfrac{\partial w}{\partial y} \end{bmatrix} \begin{bmatrix} \gamma_1 N_x^0 & 0 \\ 0 & \gamma_2 N_y^0 \end{bmatrix} \begin{bmatrix} \dfrac{\partial w}{\partial x} \\ \dfrac{\partial w}{\partial y} \end{bmatrix} \mathrm{d}\Omega \tag{34}$$

Thus the total energy functional of the hybrid laminated plates can be expressed as

$$\Pi = U_\varepsilon - W_g \tag{35}$$

3.2 Discrete system equations

The approximated discretized displacement is expressed as

$$\hat{\mathbf{u}} = \sum_{I=1}^{NP}\psi_I(x)\mathbf{u}_I \tag{36}$$

where Liu *et al*. (1995)

$$\psi_I(\boldsymbol{x}) = C(\boldsymbol{x}; \boldsymbol{x}-\boldsymbol{x}_I)\Phi_a(\boldsymbol{x}-\boldsymbol{x}_I) \tag{37}$$

$$C(\boldsymbol{x}; \boldsymbol{x}-\boldsymbol{x}_I) = \mathbf{H}^{\mathrm{T}}(\boldsymbol{x}-\boldsymbol{x}_I)\mathbf{b}(\boldsymbol{x}) \tag{38}$$

$$\begin{aligned} \mathbf{b}(\boldsymbol{x}) = [&b_0(x,y), b_1(x,y), b_2(x,y), \\ &b_3(x,y), b_4(x,y), b_5(x,y)]^{\mathrm{T}} \end{aligned} \tag{39}$$

$$\begin{aligned} \mathbf{H}^{\mathrm{T}}(\boldsymbol{x}-\boldsymbol{x}_I) = [&1, x-x_I, y-y_I, (x-x_I)(y-y_I) \\ &, (x-x_I)^2, (y-y_I)^2] \end{aligned} \tag{40}$$

Eq. (37) can be written as

$$\psi_I(\boldsymbol{x}) = \mathbf{b}^{\mathrm{T}}(\boldsymbol{x})\mathbf{H}(\boldsymbol{x}-\boldsymbol{x}_I)\Phi_a(\boldsymbol{x}-\boldsymbol{x}_I) \tag{41}$$

where

$$\mathbf{b}(\boldsymbol{x}) = \mathbf{M}^{-1}(\boldsymbol{x})\mathbf{H}(0) \tag{42}$$

$$\mathbf{B}_I(\boldsymbol{x}-\boldsymbol{x}_I) = \mathbf{H}(\boldsymbol{x}-\boldsymbol{x}_I)\Phi_a(\boldsymbol{x}-\boldsymbol{x}_I) \tag{43}$$

where

$$\mathbf{M}(\boldsymbol{x}) = \sum_{I=1}^{NP}\mathbf{H}(\boldsymbol{x}-\boldsymbol{x}_I)\mathbf{H}^{\mathrm{T}}(\boldsymbol{x}-\boldsymbol{x}_I)\Phi_a(\boldsymbol{x}-\boldsymbol{x}_I) \tag{44}$$

$$\mathbf{H}(\mathbf{0}) = [1, 0, 0, 0, 0, 0,]^{\mathrm{T}} \tag{45}$$

The kernel function $\Phi_a(x - x_I)$ is defined as

$$\Phi_a(\boldsymbol{x}-\boldsymbol{x}_I) = \Phi_a(x)\cdot\Phi_a(y) \tag{46}$$

where

$$\Phi_a(x) = \varphi\left(\frac{x-x_I}{a}\right) \tag{47}$$

The cubic spline function is selected as the weight function

$$\varphi_z(z_I)=\begin{cases}\dfrac{2}{3}-4z_I^2+4z_I^3 & \text{for } 0\le|z_I|\le\dfrac{1}{2}\\ \dfrac{4}{3}-4z_I+4z_I^2-\dfrac{4}{3}z_I^3 & \text{for } \dfrac{1}{2}<|z_I|\le 1\\ 0 & \text{otherwise}\end{cases}\tag{48}$$

The shape function thus is obtained as

$$\psi_I(\boldsymbol{x})=\mathbf{H}^{\mathrm{T}}(\mathbf{0})\mathbf{M}^{-1}(\boldsymbol{x})\mathbf{H}(\boldsymbol{x}-\boldsymbol{x}_I)\Phi_a(\boldsymbol{x}-\boldsymbol{x}_I)\tag{49}$$

According to Eq. (41), the first derivative of the shape function is presented as

$$\psi_{I,x}(\boldsymbol{x})=\mathbf{b}^{\mathrm{T}}{}_{,x}(\boldsymbol{x})\mathbf{B}_I(\boldsymbol{x}-\boldsymbol{x}_I)+\mathbf{b}^{\mathrm{T}}(\boldsymbol{x})\mathbf{B}_{I,x}(\boldsymbol{x}-\boldsymbol{x}_I)\tag{50}$$

Eq. (42) can be rewritten as

$$\mathbf{M}(\boldsymbol{x})\mathbf{b}(\boldsymbol{x})=\mathbf{H}(0)\tag{51}$$

Then

$$\mathbf{M}_{,x}(\boldsymbol{x})\mathbf{b}(\boldsymbol{x})+\mathbf{M}(\boldsymbol{x})\mathbf{b}_{,x}(\boldsymbol{x})=\mathbf{H}_{,x}(0)\tag{52}$$

$$\mathbf{M}(\boldsymbol{x})\mathbf{b}_{,x}(\boldsymbol{x})=\mathbf{H}_{,x}(0)-\mathbf{M}_{,x}(\boldsymbol{x})\mathbf{b}(\boldsymbol{x})\tag{53}$$

Therefore, the first derivative of the shape function is determined. With the same procedure, other order derivative of the shape function can also be obtained.

Generalized displacement $\tilde{\mathbf{u}}$ is defined as

$$\tilde{\mathbf{u}}_J=\hat{\mathbf{u}}(x_J)=\sum_{I=1}^{NP}L_{IJ}\mathbf{u}_I\tag{54}$$

$$L_{IJ}=\psi_I(x_J)\tag{55}$$

Then

$$\mathbf{u}=\sum_{I=1}^{NP}L_{IJ}^{-\mathrm{T}}\tilde{\mathbf{u}}_I\tag{56}$$

Substituting Eq. (56) into Eq. (54) leads to

$$\hat{\mathbf{u}}_J=\sum_{I=1}^{NP}\psi_I(x_J)\mathbf{u}_I=\sum_{I=1}^{NP}\sum_{K=1}^{NP}\psi_I(x)L_{KI}^{-\mathrm{T}}\tilde{\mathbf{u}}_K=\sum_{K=1}^{NP}\hat{\psi}_K(x)\tilde{\mathbf{u}}_K\tag{57}$$

where

$$\hat{\psi}_K(x)=\sum_{I=1}^{NP}L_{KI}^{-\mathrm{T}}\psi_I(x)\tag{58}$$

Note that

$$\hat{\psi}_I(x_J)=\sum_{I=1}^{NP}L_{IK}^{-\mathrm{T}}\psi_K(x_J)=\sum_{I=1}^{NP}L_{IK}^{-\mathrm{T}}L_{KJ}=\delta_{IJ}\tag{59}$$

Substituting Eq. (36) into Eq. (35) and performing the Ritz procedure to the total energy functional, we obtain

$$\left(\mathbf{K}+\lambda\mathbf{K}_g\right)\mathbf{u}=\mathbf{0}\tag{60}$$

where

$$\mathbf{K}=\mathbf{K}^b+\mathbf{K}^m+\mathbf{K}^s,\qquad \mathbf{K}_{IJ}^b=\int_\Omega\mathbf{B}_I^{b\mathrm{T}}\mathbf{D}\mathbf{B}_J^b\mathrm{d}\Omega\tag{61}$$

$$\mathbf{K}_{IJ}^m=\int_\Omega\mathbf{B}_I^{m\mathrm{T}}\mathbf{A}\mathbf{B}_J^m\mathrm{d}\Omega+\int_\Omega\mathbf{B}_I^{m\mathrm{T}}\bar{\mathbf{B}}\mathbf{B}_J^b\mathrm{d}\Omega+\int_\Omega\mathbf{B}_I^{b\mathrm{T}}\bar{\mathbf{B}}\mathbf{B}_J^m\mathrm{d}\Omega\tag{62}$$

$$\mathbf{K}_{IJ}^s=\int_\Omega\mathbf{B}_I^{s\mathrm{T}}\mathbf{A}^s\mathbf{B}_J^s\mathrm{d}\Omega,\qquad \mathbf{K}_g=\int_\Omega\bar{\mathbf{G}}_I^{\mathrm{T}}\bar{\mathbf{N}}\bar{\mathbf{G}}_J\mathrm{d}\Omega\tag{63}$$

The stiffness matrices in Eqs. (61)-(63) are computed via the stabilized nodal integration and direct nodal integration.

$$\mathbf{K}_{IJ}^b=\sum_{L=1}^{NP}\tilde{\mathbf{B}}_I^{b\mathrm{T}}(\mathbf{x}_L)\mathbf{D}\tilde{\mathbf{B}}_J^b(\mathbf{x}_L)A_L\tag{64}$$

$$\mathbf{K}_{IJ}^m=\sum_{L=1}^{NP}\begin{bmatrix}\mathbf{B}_I^{m\mathrm{T}}(\mathbf{x}_L)\mathbf{A}\mathbf{B}_J^m(\mathbf{x}_L)+\mathbf{B}_I^{m\mathrm{T}}(\mathbf{x}_L)\bar{\mathbf{B}}\mathbf{B}_J^b(\mathbf{x}_L)\\+\mathbf{B}_I^{b\mathrm{T}}(\mathbf{x}_L)\bar{\mathbf{B}}\mathbf{B}_J^m(\mathbf{x}_L)\end{bmatrix}A_L\tag{65}$$

$$\mathbf{K}_{IJ}^s=\sum_{L=1}^{NP}\mathbf{B}_I^{s\mathrm{T}}(\mathbf{x}_L)\mathbf{A}^s\mathbf{B}_J^s(\mathbf{x}_L)A_L\tag{66}$$

$$\mathbf{K}^g=\sum_{L=1}^{NP}\bar{\mathbf{G}}_I^{\mathrm{T}}(\mathbf{x}_L)\bar{\mathbf{N}}\bar{\mathbf{G}}_J(\mathbf{x}_L)A_L\tag{67}$$

where

$$\tilde{\mathbf{B}}_I^b(\mathbf{x}_L)=\begin{bmatrix}0&0&0&\tilde{b}_{Ix}(\mathbf{x}_L)&0\\0&0&0&0&\tilde{b}_{Iy}(\mathbf{x}_L)\\0&0&0&\tilde{b}_{Iy}(\mathbf{x}_L)&\tilde{b}_{Ix}(\mathbf{x}_L)\end{bmatrix}\tag{68}$$

$$\begin{aligned}\tilde{b}_{Ix}(\mathbf{x}_L)&=\frac{1}{A_L}\int_{\Gamma_L}\tilde{\Phi}_I(\mathbf{x}_L)n_x(\mathbf{x}_L)\mathrm{d}\Gamma\\ \tilde{b}_{Iy}(\mathbf{x}_L)&=\frac{1}{A_L}\int_{\Gamma_L}\tilde{\Phi}_I(\mathbf{x}_L)n_y(\mathbf{x}_L)\mathrm{d}\Gamma\end{aligned}\tag{69}$$

$$\mathbf{B}_I^b(\mathbf{x}_L)=\begin{bmatrix}0&0&0&\dfrac{\partial\tilde{\Phi}_I(\mathbf{x}_L)}{\partial x}&0\\0&0&0&0&\dfrac{\partial\tilde{\Phi}_I(\mathbf{x}_L)}{\partial y}\\0&0&0&\dfrac{\partial\tilde{\Phi}_I(\mathbf{x}_L)}{\partial y}&\dfrac{\partial\tilde{\Phi}_I(\mathbf{x}_L)}{\partial x}\end{bmatrix}\tag{70}$$

$$\bar{\mathbf{G}}(\mathbf{x}_L)=\begin{bmatrix}0&0&\dfrac{\partial\tilde{\Phi}_I(\mathbf{x}_L)}{\partial x}&0&0\\0&0&\dfrac{\partial\tilde{\Phi}_I(\mathbf{x}_L)}{\partial y}&0&0\end{bmatrix}\tag{71}$$

$$\mathbf{B}_I^s(\mathbf{x}_L)=\begin{bmatrix}0&0&\dfrac{\partial\tilde{\Phi}_I(\mathbf{x}_L)}{\partial x}&\tilde{\Phi}_I(\mathbf{x}_L)&0\\0&0&\dfrac{\partial\tilde{\Phi}_I(\mathbf{x}_L)}{\partial y}&0&\tilde{\Phi}_I(\mathbf{x}_L)\end{bmatrix}\tag{72}$$

$$\bar{\mathbf{N}} = \begin{bmatrix} \gamma_1 \bar{N}_{xx} & 0 \\ 0 & \gamma_2 \bar{N}_{yy} \end{bmatrix} \tag{73}$$

$$\bar{\mathbf{G}}(\mathbf{x}_L) = \begin{bmatrix} 0 & 0 & \dfrac{\partial \psi_I(\mathbf{x}_L)}{\partial x} & 0 & 0 \\ 0 & 0 & \dfrac{\partial \psi_I(\mathbf{x}_L)}{\partial y} & 0 & 0 \end{bmatrix} \tag{74}$$

4. Numerical results and discussion

Numerical results are presented in this section for buckling of hybrid laminated plates. First, it is needed to determine the effective material properties of FRC and CNTR-FG. It is assumed that FRC and CNTR-FG have the same matrix material. For the FRC ply, the volume fraction of graphite fibers is 0.6, and the material properties of which are: $E_{11}^f = 233.05$ GPa, $E_{22}^f = 23.1$ GPa, $G_{12}^f = 8.96$ GPa and $v^f = 0.2$. In addition, we assume that the out-plane shear moduli $G_{12} = G_{13}$ and $G_{23} = 1.2G_{13}$. In this study, the boundary conditions are movable and defined as

Simply supported (S):

At $x = 0, a$: $v_0 = w_0 = \phi_y = 0$,
At $y = 0, b$: $u_0 = w_0 = \phi_x = 0$.

Clamped (C):

At x=0, a: $v_0 = w_0 = \phi_x = \phi_y = 0$,
At y=0, b: $u_0 = w_0 = \phi_x = \phi_y = 0$.

Firstly, buckling analysis N_c/N_u of cracked four-layered laminates [0°/90°/90°/0°] made of graphite/epoxy material for the case $\beta_0 = 0.5$, $\beta_{90} = 0.5$ is provided to demonstrate the validity and accuracy of the proposed method. The material properties of the plate are $E_1 = 132.4$ GPa, $E_1 = E_3 = 10.8$ GPa, $G_{12} = G_{13} = 5.65$ GPa, $v_{12} = v_{13} = 0.24$ and $v_{12} = 0.49$. β_0 and β_{90} refer to the average crack densities of the 0° and 90° layers, respectively. The results for the cracked laminates are given relative to the uncracked case by considering the ratio N_c/N_u, where N_c and N_u denote the buckling loads of the cracked laminate and the corresponding uncracked laminate. As shown in Table 1, it can be seen that the present results are in good agreement

Table 1 N_c/N_u of cracked four-layered laminates [0°/90°/90°/ 0°] made of graphite/epoxy material for the case $\beta_0 = 0.5$, $\beta_{90} = 0.5$ ($\gamma_2/\gamma_1 = 0$)

a/b	$\gamma_2/\gamma_1 = 0$		$\gamma_2/\gamma_1 = 0$	
	Present	Adali and Makins (1991)	Present	Adali and Makins (1991)
0.5	0.9815	0.980	0.9195	0.918
0.6	0.9716	0.972	0.9069	0.885
0.8	0.9550	0.948	0.9346	0.936
1.0	0.9369	0.918	0.9331	0.918

Table 2 $\bar{N}_c$ and $\bar{N}_u$ for cracked and uncracked various types of [$0^C/90^F/90^F/0^C$] plates (a/b = 1.0, b/h = 10) under uniaxial compression ($\gamma_1 = -1$, $\gamma_2 = 0$) in different CNT volume fraction and boundary conditions

	CNT pattern	V_{CNT}	Buckling load parameter				
			SSSS	CCCC	SCSC	SFSF	CFCF
$\bar{N}_c$	UD	0.11	23.2179	31.2386	28.5327	9.6292	21.0273
		0.14	27.8623	38.4769	35.4991	13.1466	27.1022
		0.17	32.9307	42.9094	40.7497	18.13913	32.5435
	FG-O	0.11	22.9884	29.6411	28.2712	9.3763	20.7371
		0.14	27.6073	38.4102	35.2942	12.8336	26.8327
		0.17	32.8958	42.7429	40.3914	17.9214	31.9204
	FG-X	0.11	23.4255	31.4890	28.8524	10.0285	21.3515
		0.14	28.2521	38.8921	35.9744	13.5022	27.5637
		0.17	33.6920	43.9955	41.7976	18.7246	33.4677
$\bar{N}_u$	UD	0.11	24.6944	37.0834	36.2528	10.7975	24.9055
		0.14	29.4604	44.6355	40.0449	14.4634	31.3578
		0.17	35.0677	49.8939	46.3960	19.9510	37.7317
	FG-O	0.11	24.4436	36.8354	36.0258	10.5260	24.5486
		0.14	29.1622	44.4823	39.7208	14.1139	31.0038
		0.17	34.9302	49.6083	45.8018	19.6313	36.9836
	FG-X	0.11	24.9752	37.4030	36.5466	11.0727	25.2897
		0.14	29.8796	45.1117	40.6135	14.8459	31.8791
		0.17	35.8452	51.0031	47.5055	20.5579	38.6842

Table 3 $\bar{N}_c$ and $\bar{N}_u$ for cracked and uncracked various types of [$0^C/90^F/90^F/0^C$] plates (a/b = 1.0, b/h = 10) under biaxial compression (γ_1 = –1, γ_2 = –1) in different CNT volume fraction and boundary conditions

	CNT pattern	V_{CNT}	Buckling load parameter				
			SSSS	CCCC	SCSC	SFSF	CFCF
$\bar{N}_c$	UD	0.11	11.9237	24.3546	19.4507	4.7586	9.7930
		0.14	14.2311	29.2054	22.9443	6.3824	12.3350
		0.17	16.8149	32.4075	25.7653	8.4272	14.2495
	FG-O	0.11	11.8048	22.9669	19.2931	4.6571	9.6858
		0.14	14.0982	29.1097	22.8517	6.2602	12.2344
		0.17	16.7809	32.0398	25.5991	8.3626	13.9492
	FG-X	0.11	12.2231	24.5527	19.6113	4.8662	9.9187
		0.14	14.4285	29.5138	23.1795	6.5345	12.5218
		0.17	17.1920	33.1220	26.3092	8.6925	14.6442
$\bar{N}_u$	UD	0.11	12.5697	26.5760	20.1975	5.4385	11.5799
		0.14	14.9547	31.4359	23.6934	7.1353	14.2175
		0.17	17.7804	34.9125	26.7674	9.3602	16.2377
	FG-O	0.11	12.4425	26.3991	20.0826	5.3297	11.4552
		0.14	14.8025	31.3165	23.5971	7.0003	14.1121
		0.17	17.7061	34.6337	26.4485	9.2647	16.1162
	FG-X	0.11	12.7117	26.7945	20.3485	5.5556	11.7213
		0.14	15.1661	31.7497	23.9436	7.2976	14.4111
		0.17	18.1684	35.5979	27.3104	9.6333	16.7170

with Adali and Makins (1991) based on the classical thin plate theory.

After demonstrating the accuracy of the proposed method, numerical simulations are performed to examine the effects of CNT volume fraction, CNT distribution, plate length-to-thickness, plate aspect ratio, No. of layers, and boundary conditions on the buckling load parameters. For convenience and generality, the following non-dimensional parameters are introduced in the study: $\bar{N}_c = N_c\, b^2/(64E_m h_0^3)$ and $\bar{N}_u = N_u\, b^2/(64E_m h_0^3)$.

In Table 2, buckling load parameter $\bar{N}_c$ and $\bar{N}_u$ for cracked and uncracked various types of cross-ply [$0^C/90^F/90^F/0^C$] hybrid laminated plates (a/b = 1.0, b/h = 10) under uniaxial compression (γ_1 = –1, γ_2 = 0) in different CNT volume fraction and boundary conditions is presented.

Superscripts C and F denote CNTRC layer and FRC layer, respectively. The matrix crack density for is expressed NTR-FG layer and FRC layer by β^C and β^F.

In the present study, the value for β^C and β^F is selected as β^C = 0 and β^F = 0.5.The corresponding results of cracked and uncracked cross-ply [$0^C/90^F/90^F/0^C$] hybrid laminated plates under biaxial compression (γ_1 = –1, γ_2 = –1) is listed in Table 3. It is observed from the results that the buckling load parameters $\bar{N}_c$ and $\bar{N}_u$ for cracked and uncracked various types of cross-ply [$0^C/90^F/90^C/0^F$] hybrid laminated plates increases with the increase of CNT volume fraction, and the buckling load parameters $\bar{N}_c$ and $\bar{N}_u$ under uniaxial compression (γ_1 = –1, γ_2 = 0) are larger than those under biaxial compression (γ_1 = –1, γ_2 = –1).

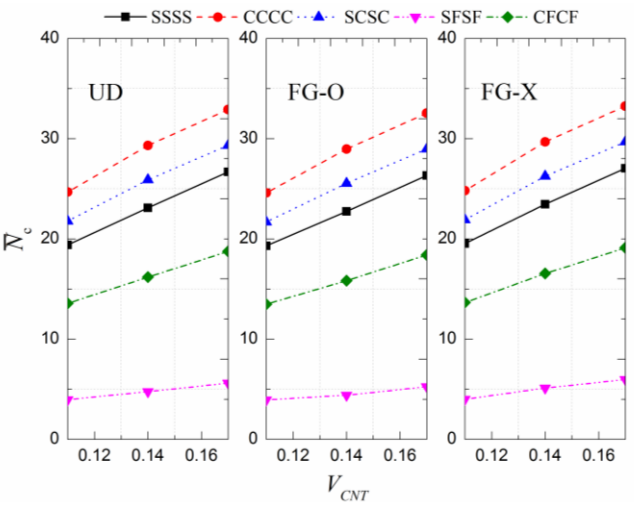

Fig. 2 $\bar{N}_c$ for cracked various types of [$45^C/-45^F/45^C/-45^F$] hybrid laminated plates (a/b = 1.0, b/h = 10) under biaxial compression (γ_1 = –1, γ_2 = –1) in different CNT volume fraction and boundary conditions

Furthermore, effect of CNT volume fraction on buckling load parameters $\bar{N}_c$ and $\bar{N}_u$ for cracked and uncracked angle-ply [$45^C/-45^F/45^C/-45^F$] hybrid laminated plates (a/b = 1, b/h = 10) under biaxial compression (γ_1 = –1, γ_2 = –1) with different boundary conditions is presented in Figs. 2-3.

Tables 4 and 5 show the buckling load parameters $\bar{N}_c$ and $\bar{N}_u$ for cracked and uncracked various types of cross-

Table 4 $\bar{N}_c$ and $\bar{N}_u$ for cracked and uncracked various types of $[0^C/90^F/90^F/0^C]$ plates (a/b = 1.0) under uniaxial compression (γ_1 = –1, γ_2 = 0) in different length-to-thickness ratio and boundary conditions

	CNT pattern	a/h	Buckling load parameter				
			SSSS	CCCC	SCSC	SFSF	CFCF
$\bar{N}_c$	UD	10	23.2179	31.2386	28.5327	9.6292	21.0273
		20	30.6169	71.8806	54.1852	12.0976	38.0636
		50	33.4838	108.4726	72.7975	13.0452	49.2838
	FG-O	10	22.9884	29.6411	28.2712	9.3763	20.7371
		20	30.2342	70.7145	53.1167	11.7022	37.0730
		50	33.0331	106.4985	71.0608	12.5851	47.6128
	FG-X	10	23.4255	31.4890	28.8524	10.0285	21.3515
		20	31.0280	73.1651	55.2687	12.4954	39.0745
		50	33.9605	110.4784	74.2103	13.5065	50.9605
$\bar{N}_u$	UD	10	24.6944	37.0834	36.2528	10.7975	24.9055
		20	31.8848	80.4605	59.1687	13.1818	42.7365
		50	34.6760	114.1441	77.5587	14.0590	53.4970
	FG-O	10	24.4436	36.8354	36.0258	10.5260	24.5486
		20	31.4916	78.5248	58.0954	12.7757	41.6565
		50	34.2233	112.2212	75.6005	13.5971	51.7982
	FG-X	10	24.9752	37.4030	36.5466	11.0727	25.2897
		20	32.3059	80.8547	60.2848	13.5896	43.8307
		50	35.1548	116.1218	79.5214	14.5218	55.2005

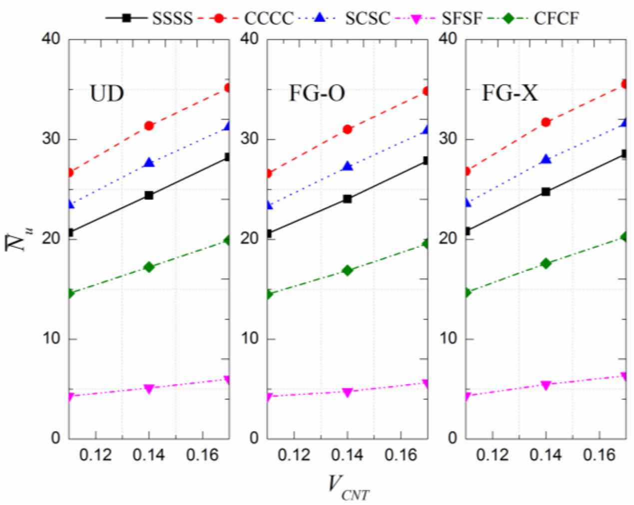

Fig. 3 $\bar{N}_u$ for uncracked various types of $[45^C/-45^F/45^C/-45^F]$ hybrid laminated plates (a/b = 1.0, b/h = 10) under biaxial compression (γ_1 = –1, γ_2 = –1) in different CNT volume fraction and boundary conditions

ply $[0^C/90^F/90^F/0^C]$ hybrid laminated plates (a/b=1.0) under uniaxial compression (γ_1 = –1, γ_2 = 0) and biaxial compression (γ_1 = –1, γ_2 = –1) in different plate length-to-thickness ratio (a/h) and boundary conditions. It is evident that as the boundary condition changes from the fully clamped to simply- supported and/or free for the corresponding support edges, for example from CCCC to SFSF, the buckling load parameter becomes lower.

This is because a higher constraint at the edge increases the plate flexural rigidity, resulting in a higher buckling load. It is found that with the increase of plate length-to-thickness ratio, the buckling load parameters increase. Effect of plate length-to-thickness ratio (a/h) on buckling load parameters $\bar{N}_c$ and $\bar{N}_u$ for cracked and uncracked various types of angle-ply $[45^C/-45^F/45^C/-45^F]$ hybrid laminated plates (a/b = 1.0) under biaxial compression (γ_1 = –1, γ_2 = –1) are presented in Figs. 4-5.

The effect of plate aspect ratio a/b on the buckling load parameters $\bar{N}_c$ and $\bar{N}_u$ for cracked and uncracked various types of cross-ply $[0^C/90^F/90^F/0^C]$ hybrid laminated plates (b/h = 10) under uniaxial compression (γ_1 = –1, γ_2 = 0) and biaxial compression (γ_1 = –1, γ_2 = –1) are given in Tables 6 and 7. It can be seen that the buckling load parameters $\bar{N}_c$ and $\bar{N}_u$ decrease with the increasing thickness ratio. For hybrid laminated plates containing UD, FG-O and FG-X types of CNTR-FG layers. We can also observe that the buckling load parameters $\bar{N}_c$ and $\bar{N}_u$ for FG-O hybrid laminated plates is a little lower than UD hybrid laminated plates, while that of FG-X hybrid laminated plates is a little higher than UD hybrid laminated plates. Effect of plate aspect ratio on buckling load parameters $\bar{N}_c$ and $\bar{N}_u$ for cracked and uncracked various types of angle-ply $[45^C/-45^F/45^C/-45^F]$ hybrid laminated plates (b/h = 10) under uniaxial compression (γ_1 = –1, γ_2 = 0) and biaxial compression (γ_1 = –1, γ_2 = –1)

Table 5 $\overline{N}_c$ and $\overline{N}_u$ for cracked and uncracked various types of [$0^C/90^F/90^F/0^C$] plates (a/b = 1.0) under biaxial compression (γ_1 = –1, γ_2 = –1) in different length-to-thickness ratio and boundary conditions

	CNT pattern	a/h	Buckling load parameter				
			SSSS	CCCC	SCSC	SFSF	CFCF
$\overline{N}_c$	UD	10	11.9237	24.3546	19.4507	4.7586	9.7930
		20	15.3955	45.9124	35.1378	6.0065	18.2937
		50	16.7678	61.0135	46.2914	6.4984	24.1163
	FG-O	10	11.8048	22.9669	19.2931	4.6571	9.6858
		20	15.2040	45.3998	34.9702	5.8372	17.8768
		50	16.5427	60.1694	46.0969	6.2983	23.4008
	FG-X	10	12.2231	24.5527	19.6113	4.8662	9.9187
		20	15.6013	46.4718	35.3511	6.1804	18.7231
		50	17.0058	61.8957	46.5324	6.7026	24.8898
$\overline{N}_u$	UD	10	12.5697	26.5760	20.1975	5.4385	11.5799
		20	16.0178	48.4958	35.7815	6.6886	20.6216
		50	17.3616	63.3297	46.9014	7.1596	26.3523
	FG-O	10	12.4425	26.3991	20.0826	5.3297	11.4552
		20	15.8213	47.9532	35.6125	6.5144	20.1768
		50	17.1355	62.4712	46.7072	6.9587	25.6058
	FG-X	10	12.7117	26.7945	20.3485	5.5556	11.7213
		20	16.2283	49.0847	35.9971	6.8671	21.0762
		50	17.6007	64.2320	47.1363	7.3649	27.1011

Table 6 $\overline{N}_c$ and $\overline{N}_u$ for cracked and uncracked various types of [$0^C/90^F/90^F/0^C$] laminated plates (b/h = 10) under uniaxial compression (γ_1 = –1, γ_2 = 0) in different plate aspect ratio and boundary conditions

	CNT pattern	a/h	Buckling load parameter				
			SSSS	CCCC	SCSC	SFSF	CFCF
$\overline{N}_c$	UD	1	23.2179	31.2386	28.5327	9.6292	21.0273
		1.25	22.9097	30.5856	28.4860	6.8282	17.1423
		1.5	22.0858	30.3744	28.4542	5.0400	13.9849
	FG-O	1	22.9884	29.6411	28.2712	9.3763	20.7371
		1.25	22.5950	29.6131	28.1402	6.6320	16.8345
		1.5	21.8068	29.0152	28.2064	4.8864	13.6867
	FG-X	1	23.4255	31.4890	28.8524	10.0285	21.3515
		1.25	23.2396	30.9144	28.6967	7.0270	17.4705
		1.5	22.3946	30.6790	28.6569	5.1964	14.2954
$\overline{N}_u$	UD	1	24.6944	37.0834	36.2528	10.7975	24.9055
		1.25	24.3610	35.6309	34.1802	7.5683	19.9332
		1.5	24.2759	34.9852	32.4299	5.5415	16.0237
	FG-O	1	24.4436	36.8354	36.0258	10.5260	24.5486
		1.25	23.9986	35.3251	31.5384	7.3594	19.5707
		1.5	23.9533	34.6853	32.1361	5.5481	15.6841
	FG-X	1	24.9752	37.4030	36.5466	11.0727	25.2897
		1.25	24.8321	35.9922	34.7738	7.7789	20.3111
		1.5	24.6248	35.3430	32.7769	5.7040	16.3725

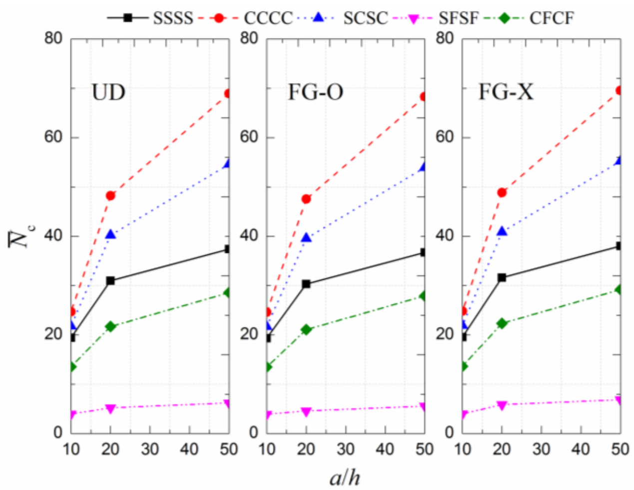

Fig. 4 $\bar{N}_c$ for cracked various types of [45^C/-45^F/45^C/-45^F] laminated plates (a/b = 1.0) under biaxial compression ($\gamma_1 = -1$, $\gamma_2 = -1$) in different plate length-to-thickness ratio and boundary conditions

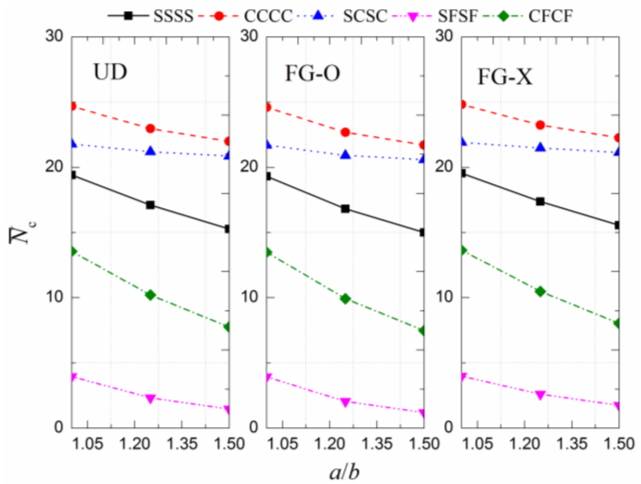

Fig. 6 $\bar{N}_c$ for cracked various types of angle-ply [45^C/-45^F/45^C/-45^F] hybrid laminated plates (a/b = 1) under biaxial compression ($\gamma_1 = -1$, $\gamma_2 = -1$) in different No. of layers and boundary conditions

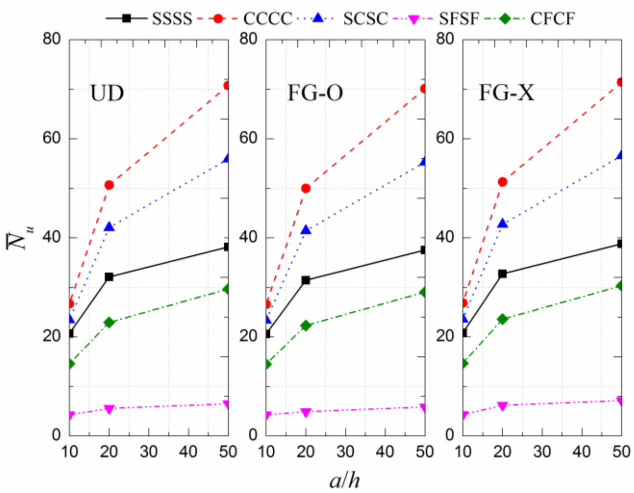

Fig. 5 $\bar{N}_u$ for uncracked various types of [45^C/-45^F/45^C/-45^F] laminated plates (a/b = 1.0) under biaxial compression ($\gamma_1 = -1$, $\gamma_2 = -1$) in different plate length-to-thickness ratio and boundary conditions

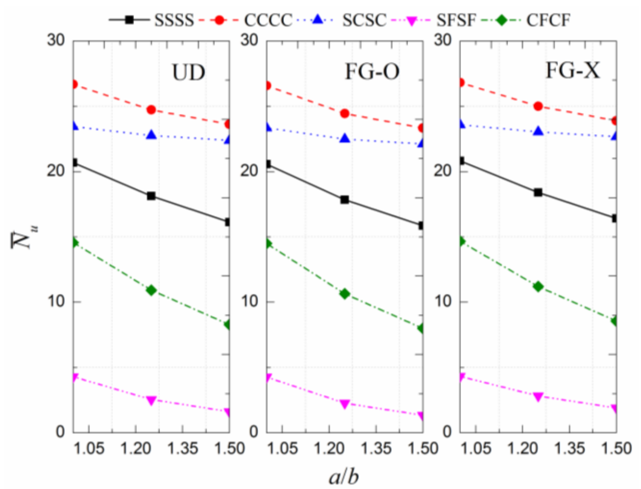

Fig. 7 $\bar{N}_u$ for uncracked various types of angle-ply [45^C/-45^F/45^C/-45^F] hybrid laminated plates (a/b = 1) under biaxial compression ($\gamma_1 = -1$, $\gamma_2 = -1$) in different No. of layers and boundary conditions

under different boundary conditions are presented in Figs. 6-7.

Buckling load parameters $\bar{N}_c$ and $\bar{N}_u$ for cracked and uncracked various types of cross-ply [...0^C/90^F/90^F/0^C...] hybrid laminated plates (a/b = 1) under uniaxial compression ($\gamma_1 = -1$, $\gamma_2 = 0$) and biaxial compression ($\gamma_1 = -1$, $\gamma_2 = -1$) in different No. of layers and boundary conditions are presented in Tables 8 and 9. It can be seen that the buckling load parameters $\bar{N}_c$ and $\bar{N}_u$ increase quickly with the increase of No. of layers. Effect of No. of layers on buckling load $\bar{N}_c$ and $\bar{N}_u$ for cracked and uncracked various types of angle-ply [...45^C/-45^F/45^C/-45^F...] hybrid laminated plates (a/b=1) under uniaxial compression ($\gamma_1 = -1$, $\gamma_2 = 0$) and biaxial compression ($\gamma_1 = -1$, $\gamma_2 = -1$) are illustrated in Figs. 8 and 9. It can be seen that the buckling load parameters $\bar{N}_c$ for cracked hybrid laminated plates are lower than $\bar{N}_u$ for uncracked hybrid laminated plates. That is because the introduction of matrix crack leads the reduction of the stiffness of the hybrid laminated plates.

5. Conclusions

In this study, the buckling behavior of a hybrid laminated plates containing CNTR-FG layers is studied. The cracks are modeled as aligned slit cracks across the ply thickness and transverse to the laminate plane, and the

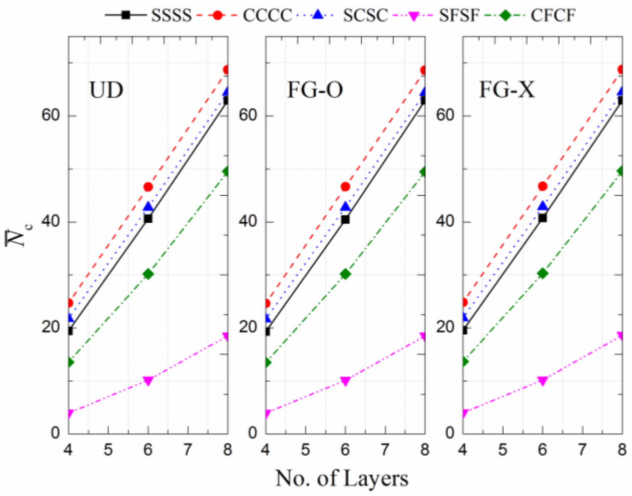

Fig. 8 $\bar{N}_c$ for cracked various types of angle-ply [...45^C/-45^F/45^C/-45^F...] hybrid laminated plates (a/b = 1) under biaxial compression (γ_1 = –1, γ_2 = –1) in different No. of layers and boundary conditions

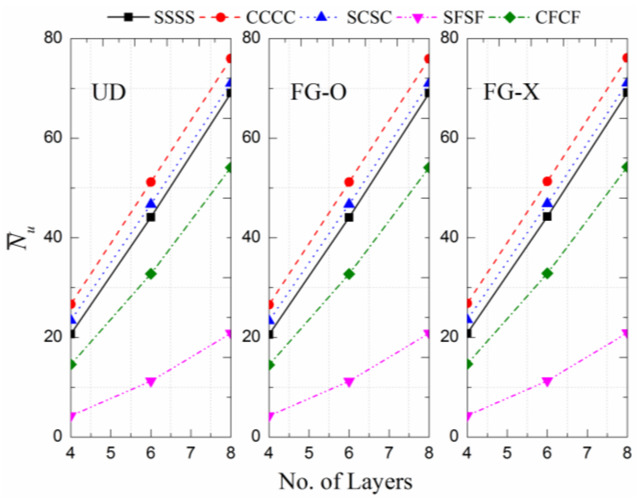

Fig. 8 $\bar{N}_u$ for uncracked various types of angle-ply [...45^C/-45^F/45^C/-45^F...] hybrid laminated plates (a/b = 1) under biaxial compression (γ_1 = –1, γ_2 = –1) in different No. of layers and boundary conditions

distribution of cracks is assumed to be statistically homogeneous corresponding to an average crack density. The formulation of the governing eigenvalue problem is based on the first-order shear deformation theory and the kp-Ritz method. Detailed parametric studies are presented to investigate the effect matrix crack density, CNTs distributions, CNT volume fraction, plate aspect ratio and plate length-to-thickness ratio, boundary conditions and number of layers on buckling behaviors of hybrid laminated plates.

Table 7 $\bar{N}_c$ and $\bar{N}_u$ for cracked and uncracked various types of [0^C/90^F/90^F/0^C] laminated plates (b/h = 10) under uniaxial compression (γ_1 = –1, γ_2 = 0) in different plate aspect ratio and boundary conditions

	CNT pattern	*a*/*b*	Buckling load parameter				
			SSSS	CCCC	SCSC	SFSF	CFCF
$\bar{N}_c$	UD	1	11.9237	24.3546	19.4507	4.7586	9.7930
		1.25	11.2010	23.1159	19.2286	2.7530	6.436
		1.5	11.1488	22.4098	18.9102	1.6935	4.2766
	FG-O	1	11.8048	22.9669	19.2931	4.6571	9.6858
		1.25	11.1321	22.9735	18.7484	2.6910	6.3425
		1.5	11.1086	22.2661	18.7347	1.6553	4.2020
	FG-X	1	12.2231	24.5527	19.6113	4.8662	9.9187
		1.25	11.2854	23.3020	19.4133	2.8185	6.5406
		1.5	11.2048	22.5879	19.1268	1.7339	4.3572
$\bar{N}_u$	UD	1	12.5697	26.5760	20.1975	5.4385	11.5799
		1.25	11.5502	24.6643	19.7331	3.1417	7.5527
		1.5	11.3796	23.8123	19.4060	1.9365	4.9775
	FG-O	1	12.4425	26.3991	20.0826	5.3297	11.4552
		1.25	11.4765	24.4376	19.6377	3.0759	7.4436
		1.5	11.3180	23.6784	19.3211	1.8967	4.8925
	FG-X	1	12.7117	26.7945	20.3485	5.5556	11.7213
		1.25	11.6391	24.8794	19.8651	3.2110	7.6707
		1.5	11.4102	23.9948	19.6112	1.9787	5.0676

Table 8 $\bar{N}_c$ and $\bar{N}_u$ for cracked and uncracked various types of [...$0^C/90^F/90^F/0^C$...] laminated plates (a/b = 1) under uniaxial compression (γ_1 = –1, γ_2 = 0) in different No. of layers and boundary conditions

	CNT pattern	No. of layers	Buckling load parameter				
			SSSS	CCCC	SCSC	SFSF	CFCF
$\bar{N}_c$	UD	4	23.2179	31.2386	28.5327	9.6292	21.0273
		6	49.9678	53.4714	51.2591	25.6613	41.7122
		8	69.7656	75.8935	72.1640	44.7641	61.6297
	FG-O	4	22.9884	29.6411	28.2712	9.3763	20.7371
		6	49.9515	53.3742	51.2041	25.4937	41.6450
		8	69.7281	75.7979	72.1450	44.6892	61.5842
	FG-X	4	23.4255	31.4890	28.8524	10.0285	21.3515
		6	50.1357	53.5906	51.3695	25.8735	41.8995
		8	69.9104	75.9790	72.2402	44.9445	61.7911
$\bar{N}_u$	UD	4	24.6944	37.0834	36.2528	10.7975	24.9055
		6	59.6926	65.8884	62.9912	29.4809	50.7872
		8	87.3936	91.8606	89.1257	52.7912	76.2287
	FG-O	4	24.4436	36.8354	36.0258	10.5260	24.5486
		6	59.5958	65.8809	62.8142	29.2740	50.6729
		8	87.4848	91.6917	89.0579	52.6754	76.2046
	FG-X	4	24.9752	37.4030	36.5466	11.0727	25.2897
		6	59.9227	66.0659	63.0628	29.7240	51.0112
		8	87.5466	91.9885	89.3013	52.9980	76.4087

Table 9 $\bar{N}_c$ and $\bar{N}_u$ for cracked and uncracked various types of [...$0^C/90^F/90^F/0^C$...] hybrid laminated plates (a/b = 1) under biiaxial compression (γ_1 = –1, γ_2 = –1) in No. of layers and boundary conditions

	CNT pattern	No. of layers	Buckling load parameter				
			SSSS	CCCC	SCSC	SFSF	CFCF
$\bar{N}_c$	UD	4	11.9237	24.3546	19.4507	4.7586	9.79305
		6	30.7895	46.4778	40.3783	12.5529	19.1528
		8	52.6218	67.2803	61.9115	21.9890	28.4280
	FG-O	4	11.8048	22.9669	19.2931	4.6571	9.6858
		6	30.7272	46.3959	40.3330	12.4929	19.1410
		8	52.6204	67.2049	61.8490	21.9725	28.3991
	FG-X	4	12.2231	24.5527	19.6113	4.8662	9.9187
		6	30.9121	46.6177	40.5201	12.6407	19.2239
		8	52.7466	67.4247	62.0576	22.0666	28.4949
$\bar{N}_u$	UD	4	12.5697	26.5760	20.1975	5.4385	11.5799
		6	32.8397	52.4455	42.5706	14.6712	23.1515
		8	56.8525	77.4900	66.4972	26.2664	34.7928
	FG-O	4	12.4425	26.3991	20.0826	5.3297	11.4552
		6	32.7605	52.4181	42.5067	14.5708	23.1275
		8	56.8340	77.3783	66.4553	26.2383	34.7739
	FG-X	4	12.7117	26.7945	20.3485	5.5556	11.7213
		6	32.9785	52.5966	42.7262	14.7746	23.2316
		8	56.9891	77.6356	66.6542	26.3524	34.8634

Acknowledgments

The research described in this paper was financially supported by the National Natural Science Foundation of China (Grant no. 11702138), Natural Science Foundation of Jiangsu Province (Grant no. BK20150766 and BK20170820) and the Fundamental Research Funds for the Central Universities (no. 30916011341 and 30917011339).

References

Adali, S. and Makins, R.K. (1991), "Buckling of unsymmetrical, cross-ply laminates with matrix cracks", *Int. J. Mech. Sci.*, **33**(10), 851-861.

Arani, A.G., Kolahdouzan, F. and Abdollahian, M. (2018), "Buckling and free vibration analysis of FG-CNTRC-micro sandwich plate", *Steel Compos. Struct., Int. J.*, **26**(3), 273-287.

Asadi, H. (2017), "Numerical simulation of the fluid-solid interaction for CNT reinforced functionally graded cylindrical shells in thermal environments", *Acta Astronautica*, **138** 214-224.

Asadi, H. and Wang, Q. (2017a), "An investigation on the aeroelastic flutter characteristics of FG-CNTRC beams in the supersonic flow", *Compos. Part B: Eng.*, **116**, 486-499.

Asadi, H. and Wang, Q. (2017), "Dynamic stability analysis of a pressurized FG-CNTRC cylindrical shell interacting with supersonic airflow", *Compos. Part B: Eng.*, **118**, 15-25.

Asadi, H., Souri, M. and Wang, Q. (2017), "A numerical study on flow-induced instabilities of supersonic FG-CNT reinforced composite flat panels in thermal environments", *Compos. Struct.*, **171**, 113-125.

Bahrami, M.N., Allahkarami, F. and Saryazdi, M.G. (2018), "Nonlinear forced vibration of FG-CNTs-reinforced curved microbeam based on strain gradient theory considering out-of-plane motion", *Steel Compos. Struct., Int. J.*, **26**(6), 673-691.

Budiansky, B. and O'Connell, R.J. (1976), "Elastic moduli of a cracked solid", *Int. J. Solids Struct.*, **12**(2), 81-97.

Dvorak, G.J., Laws, N. and Hejazi, M. (1985), "Analysis of progressive matrix cracking in composite laminates I. Thermoelastic properties of a ply with cracks", *J. Compos. Mater.*, **19**(3), 216-234.

Ebrahimi, F. and Farazmandnia, N. (2018), "Thermal buckling analysis of functionally graded carbon nanotube-reinforced composite sandwich beams", *Steel Compos. Struct., Int. J.*, **27**(2), 149-159.

Efraim, E. and Eisenberger, M. (2007), "Exact vibration analysis of variable thickness thick annular isotropic and FGM plates", *J. Sound Vib.*, **299**(4-5), 720-738.

Gayathri, P., Umesh, K. and Ganguli, R. (2010), "Effect of matrix cracking and material uncertainty on composite plates", *Reliabil. Eng. Syst. Safe.*, **95**(7), 716-728.

Gudmundson, P. and Weilin, Z. (1993), "An analytic model for thermoelastic properties of composite laminates containing transverse matrix cracks", *Int. J. Solids Struct.*, **30**(23), 3211-3231.

Kashtalyan, M. and Soutis, C. (2013), "Predicting residual stiffness of cracked composite laminates subjected to multi-axial inplane loading", *J. Compos. Mater.*, **47**(20-21), 2513-2524.

Keleshteri, M.M., Asadi, H. and Wang, Q. (2017a), "Large amplitude vibration of FG-CNT reinforced composite annular plates with integrated piezoelectric layers on elastic foundation", *Thin-Wall. Struct.*, **120**, 203-214.

Keleshteri, M.M., Asadi, H. and Wang, Q. (2017b), "Postbuckling analysis of smart FG-CNTRC annular sector plates with surface-bonded piezoelectric layers using generalized differential quadrature method", *Comput. Methods Appl. Mech. Eng.*, **325**, 689-710.

Keleshteri, M.M., Asadi, H. and Wang, Q. (2018), "On the snap-through instability of post-buckled FG-CNTRC rectangular plates with integrated piezoelectric layers", *Comput. Methods Appl. Mech. Eng.*, **331**, 53-71.

Laws, N. and Dvorak, G.J. (1988), "Progressive transverse cracking in composite laminates", *J. Compos. Mater.*, **22**(10), 900-916.

Laws, N., Dvorak, G.J. and Hejazi, M. (1983), "Stiffness changes in unidirectional composites caused by crack systems", *Mech. Mater.*, **2**(2), 123-137.

Lee, J.-W. and Daniel, I.M. (1990), "Progressive transverse cracking of crossply composite laminates", *J. Compos. Mater.*, **24**(11), 1225-1243.

Lei, Z.X., Zhang, L.W. and Liew, K.M. (2016a), "Analysis of laminated CNT reinforced functionally graded plates using the element-free kp-Ritz method", *Compos. Part B: Eng.*, **84**, 211-221.

Lei, Z.X., Zhang, L.W. and Liew, K.M. (2016b), "Parametric analysis of frequency of rotating laminated CNT reinforced functionally graded cylindrical panels", *Compos. Part B: Eng.*, **90**, 251-266.

Liu, W.K., Jun, S., Li, S., Adee, J. and Belytschko, T. (1995), "Reproducing kernel particle methods for structural dynamics", *Int. J. Numer. Methods Eng.*, **38**(10), 1655-1679.

Makins, R.K. and Adali, S. (1991), "Bending of cross-ply laminated plates with matrix cracks", *J. Strain Anal. Eng. Des.*, **26**(4), 253-257.

Mehri, M., Asadi, H. and Wang, Q. (2016a), "Buckling and vibration analysis of a pressurized CNT reinforced functionally graded truncated conical shell under an axial compression using HDQ method", *Methods Appl. Mech. Eng.*, **303**, 75-100.

Mehri, M., Asadi, H. and Wang, Q. (2016b), "On dynamic instability of a pressurized functionally graded carbon nanotube reinforced truncated conical shell subjected to yawed supersonic airflow", *Compos. Struct.*, **153**, 938-951.

Mehri, M., Asadi, H. and Kouchakzadeh, M.A. (2017), "Computationally efficient model for flow-induced instability of CNT reinforced functionally graded truncated conical curved panels subjected to axial compression", *Comput. Methods Appl. Mech. Eng.*, **318**, 957-980.

Mohammadzadeh-Keleshteri, M., Asadi, H. and Aghdam, M.M. (2017), "Geometrical nonlinear free vibration responses of FG-CNT reinforced composite annular sector plates integrated with piezoelectric layers", *Compos. Struct.*, **171**, 100-112.

Moradi-Dastjerdi, R. and Payganeh, G. (2017), "Thermoelastic dynamic analysis of wavy carbon nanotube reinforced cylinders under thermal loads", *Steel Compos. Struct., Int. J.*, **25**(3), 315-326.

Nikrad, S.F. and Asadi, H. (2015), "Thermal postbuckling analysis of temperature dependent delaminated composite plates", *Thin-Wall. Struct.*, **97**, 296-307.

Nikrad, S.F., Asadi, H., Akbarzadeh, A.H. and Chen, Z.T. (2015), "On thermal instability of delaminated composite plates", *Compos. Struct.*, **132**, 1149-1159.

Nikrad, S.F., Keypoursangsari, S., Asadi, H., Akbarzadeh, A.H. and Chen, Z.T. (2016), "Computational study on compressive instability of composite plates with off-center delaminations", *Comput. Methods Appl. Mech. Eng.*, **310**, 429-459.

Nikrad, S.F., Asadi, H. and Wang, Q. (2017), "Postbuckling behaviors of open section composite struts with edge delamination using a layerwise theory", *Int. J. Non-Linear Mech.*, **95**, 315-326.

Shen, H.-S. (2009a), "A comparison of buckling and postbuckling behavior of FGM plates with piezoelectric fiber reinforced

composite actuators", *Compos. Struct.*, **91**(3), 375-384.
Shen, H.-S. (2009b), "Nonlinear bending of functionally graded carbon nanotube-reinforced composite plates in thermal environments", *Compos. Struct.*, **91**(1), 9-19.
Tahouneh, V. (2018), "3-D Vibration analysis of FG-MWCNTs/Phenolic sandwich sectorial plates", *Steel Compos. Struct., Int. J.*, **26**(5), 649-662.

CC